

# Fluorescent Triazole Urea Activity-Based Probes for the Single-Cell Phenotypic Characterization of *Staphylococcus aureus*

Linhai Chen, Laura J. Keller, Edward Cordasco, Matthew Bogyo,\* and Christian S. Lentz\*

**Abstract:** Phenotypically distinct cellular (sub)populations are clinically relevant for the virulence and antibiotic resistance of a bacterial pathogen, but functionally different cells are usually indistinguishable from each other. Herein, we introduce fluorescent activity-based probes as chemical tools for the single-cell phenotypic characterization of enzyme activity levels in *Staphylococcus aureus*. We screened a 1,2,3-triazole urea library to identify selective inhibitors of fluorophosphonate-binding serine hydrolases and lipases in *S. aureus* and synthesized target-selective activity-based probes. Molecular imaging and activity-based protein profiling studies with these probes revealed a dynamic network within this enzyme family involving compensatory regulation of specific family members and exposed single-cell phenotypic heterogeneity. We propose the labeling of enzymatic activities by chemical probes as a generalizable method for the phenotyping of bacterial cells at the population and single-cell level.

A phenotype describes the sum of observable traits of a biological specimen such as a bacterial cell. Although individual cells of an isogenic bacterial population are usually indistinguishable from each other, cells are known to functionally respond to their environment, for example, through the expression of virulence factors, and functionally distinct cellular subsets have been described. The latter phenomenon, known as phenotypic heterogeneity, becomes apparent and

clinically relevant in the formation of surface-associated bacterial communities known as biofilms,<sup>[1]</sup> the presence of persister cells,<sup>[2]</sup> or in antimicrobial heteroresistance, that is, the presence of cellular subpopulations with different susceptibilities to antibiotics.<sup>[3]</sup> However, many functional characteristics and responses of these cells remain hidden as non-observable traits unless they involve morphological changes or are visualized by some experimental method. Important insights into the phenotypic responses of bacterial pathogens to host factors or other stress or culture conditions have been gained through transcriptomic or proteomic methods.<sup>[4]</sup> Such studies are commonly performed at the level of entire cell populations, providing a phenotypic snapshot of the “averaged” cell and are thus unable to detect patterns of phenotypic heterogeneity within a population.

Activity-based probes (ABPs) are functionalized active-site-directed irreversible enzyme inhibitors that have been used in a range of diverse applications from chemoproteomic profiling and identification of enzymatic targets<sup>[5]</sup> to non-invasive in vivo imaging in living animals.<sup>[6]</sup> As molecular imaging with fluorescent ABPs can be used to visualize the localization and distribution of an enzymatic target in its physiological environment with single-cell and subcellular resolution,<sup>[7]</sup> we reasoned that this class of chemical tools may be exploited for the phenotypic characterization of native bacterial populations.

We have recently performed a cell-based chemical proteomics study in the Gram-positive opportunistic bacterial pathogen *Staphylococcus aureus* that identified 12 active serine hydrolase targets, including lipase 1 and 2 (SAL1, SAL2) as well as 10 largely uncharacterized hydrolases that we termed fluorophosphonate-binding hydrolases (Fph) A–J.<sup>[7a]</sup> The secreted *S. aureus* lipases SAL1/2 are encoded as pre-proteins by the *gehA* and *gehB* genes.<sup>[8]</sup> Both have recently been ascribed roles in bacterial virulence by promoting biofilm formation and host cell invasion.<sup>[8]</sup> Our preliminary functional characterization of Fph enzymes focused on the 34 kDa FphB. We described FphB as a virulence factor, the activity of which is regulated at the host–pathogen interface.<sup>[7a]</sup> In a systemic mouse infection model, we also found a mild contribution to liver pathogenicity for the 31 kDa hydrolase FphE.<sup>[7a]</sup> The catalytic activities and functional relevance of the other 8 Fph enzymes remain unexplored. Competitive activity-based protein profiling of fluorophosphonate (FP)-labeling in *S. aureus* using our in-house library of circa 500 serine-reactive compounds (based on chloroisocoumarin, sulfonyl fluoride, or diphenyl phosphonate electrophiles) identified a chloroisocoumarin hit that we developed into an FphB-selective fluorescent ABP. This probe provided important insight into the localization of



[\*] Dr. L. Chen, E. Cordasco, Prof. Dr. M. Bogyo, Dr. C. S. Lentz  
Stanford University School of Medicine, Department of Pathology  
300 Pasteur Drive, Stanford, CA 94305 (USA)  
E-mail: mbogyo@stanford.edu

Dr. L. Chen  
National Center for Drug Screening, State Key Laboratory of Drug Research, Shanghai Institute of Materia Medica  
Chinese Academy of Sciences  
189 Guoshoujing Road, Shanghai 201203 (China)

L. J. Keller  
Stanford University School of Medicine  
Department of Chemical & Systems Biology  
300 Pasteur Drive, Stanford, CA 94305 (USA)

Prof. Dr. M. Bogyo  
Stanford University School of Medicine  
Department of Microbiology & Immunology  
300 Pasteur Drive, Stanford, CA 94305 (USA)

Dr. C. S. Lentz  
Department of Chemical Biology  
Helmholtz-Centre for Infection Research (HZI)  
Braunschweig (Germany)  
E-mail: Christian.Lentz@helmholtz-hzi.de

 Supporting information and the ORCID identification number(s) for the author(s) of this article can be found under:  
 <https://doi.org/10.1002/anie.201900511>.

FphB in the bacterial cell envelope and its heterogenous distribution among cells of a larger bacterial population.<sup>[7a]</sup> Inspired by these results, we now aimed to develop further target-selective fluorescent probes directed against these chemically tractable serine hydrolases and to build a chemical toolkit for molecular imaging-based single-cell phenotypic analysis of bacterial populations.

In this study, we explore 1,2,3-triazole ureas (TUs) as another class of potent serine-reactive compounds to further develop ABPs for diverse members of the *S. aureus* Fphs. TUs have been shown by Cravatt and co-workers to be valuable tools for the inhibition of serine hydrolase targets and several candidates have emerged as selective inhibitors of human hydrolases with potent and selective *in vivo* activity.<sup>[9]</sup> TUs act by carbamylation of their target enzyme resulting in elimination of the triazole leaving group.<sup>[9a]</sup> Selective release of the leaving group adds additional versatility to this chemotype allowing for the design of quenched fluorescent ABPs.<sup>[10]</sup> Initially, we screened a library of circa 150 TU compounds for competition with FP-tetramethylrhodamine (FP-TMR)-labeling of serine hydrolases active in live *S. aureus* ATCC35556 grown on tryptic soy agar supplemented with MgCl<sub>2</sub> (TSAMg), as used in our previous screen<sup>[7a]</sup> and reported to be biofilm-promoting.<sup>[11]</sup> The library compounds had high activity against *S. aureus* serine hydrolases with 53 hit compounds showing greater than 50 % competition of FP-TMR labeling of at least one hydrolase target at a final concentration of 1  $\mu$ M (8 compounds exceeding this threshold at 100 nM; Figure S1). To explore the potential of these compounds for the development of target-specific inhibitors and probes, we selected four hit scaffolds with diverse selectivity profiles for re-synthesis, validation in dose-response, and target identification (Figure 1A). The carbamylation-based synthesis of TUs yields a mixture of 1,4-linked (designated as **a** throughout this work) and 2,4-linked (designated as **b**) triazoles. These regio-isomers were purified

and tested separately. The compounds were tested in dose-response against the screening strain ATCC35556 under biofilm-promoting conditions (Supporting Information, Figure S1 and S2) and also validated against the clinically relevant methicillin-resistant (MRSA) strain USA300 and the methicillin-sensitive strain Newman (Figure 1B and Figure S2, overview of all strains used in Table S1). Transposon mutants with insertions in individual *fph* genes (designated as :Tn strains) are available for both Newman and USA300, allowing rapid assignment of target identities. The screening hit **1b** (AA395) preferentially blocked FP-TMR labeling of FphB (IC<sub>50</sub> = 128 nM) with a circa 4–5-fold selectivity over the approximately 50 kDa FphA as a secondary target (Figure 1B and Figure S2A,B), while its 1,4-regioisomer **1a** also targeted a greater than 66.5 kDa and an approximately 40 kDa hydrolase (IC<sub>50</sub>  $\approx$  19 nM), assigned to the pro-protein and matured form of SAL1 or SAL2 (Figure 1B and Figure S2A,B). Validation of the other hit compounds revealed diverse target selectivity profiles, most notably compounds **2b** and **3a** have a similar labeling profile and preferentially target both FphA and FphH, whereas compounds **4a/b** (KT129/KT130) showed selectivity for the 29 kDa hydrolase FphF (Figure 1B and Figure S2, see Supplementary Results in the Supporting Information for a detailed description of the selectivity profiles and structure–activity relationship).

To convert these inhibitors into fluorescent ABPs, we focused on analogs of **1a** and **1b** as their reactivity profile suggested they might yield potent fluorescent ABPs for FphB and open a pathway to generate quenched fluorescent probes for this target. Furthermore, structural modifications may switch the selectivity profile and generate specificity for secondary targets of the parent inhibitor. We synthesized a series of clickable analogs (**5–7a/b**) in which an alkyne handle was installed after a C<sub>2</sub> (**5,6**) or PEG<sub>3</sub> linker (**7**) replacing the pyrrolidinyl substituent of the parent compound. In order to generate a secondary amine as present in

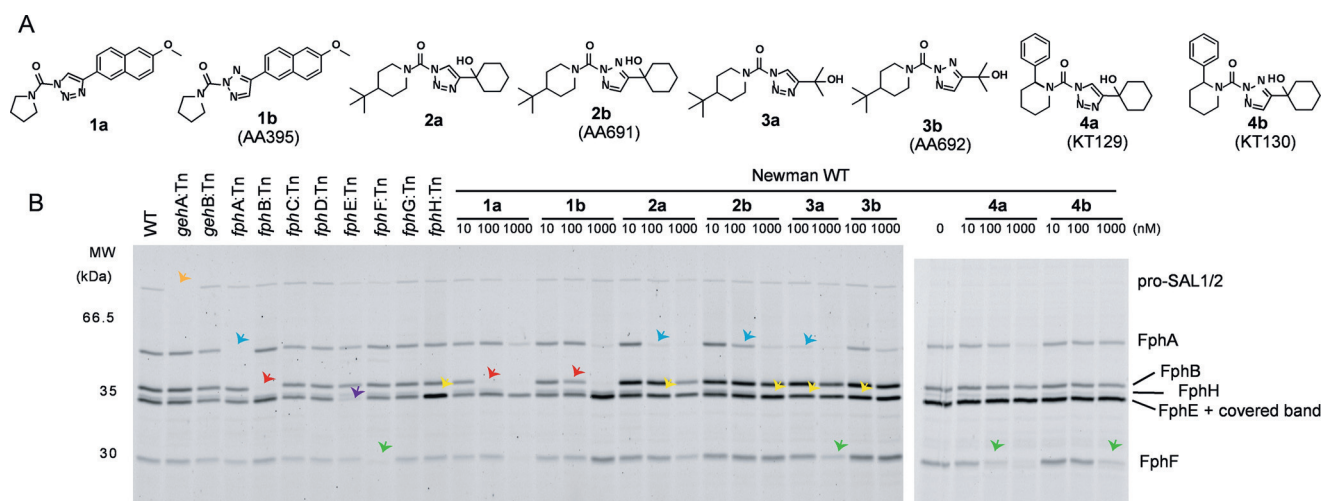


**Figure 1.** Inhibitory profile of TU screening hits and labeling profile of clickable probes. A) Chemical structures of hit compounds and their regioisomers **1–4 a/b**. B) Competitive FP-TMR labelling profiles of *S. aureus* Newman WT or indicated transposon mutant (:Tn) strains after preincubation with compounds **1–4 a/b**. Cells were harvested from TSAMg plates, preincubated with inhibitors for 60 min, labelled with FP-TMR (1  $\mu$ M), lysed, and analysed by SDS-PAGE/fluorescence scan. Preferred targets of each probe (according to transposon mutant analysis) are highlighted by colored arrows: Orange = SAL1, blue = FphA, red = FphB, green = FphF, yellow = FphH, and purple = FphE.

the pyrrolidinyl substituent of **1**, compounds **6** and **7** feature an additional propyl substituent (Figure 2A). Alkyne probes **6** and **7** could easily be converted into fluorescent ABPs through copper-catalyzed azide–alkyne cycloaddition with a bodipyTMR dye leading to probes **8a/b** and **9a/b**, respectively. In contrast, our attempts to synthesize fluorescent analogs of probes **5a/b** by this method failed owing to the decomposition of the primary amine triazole urea group.

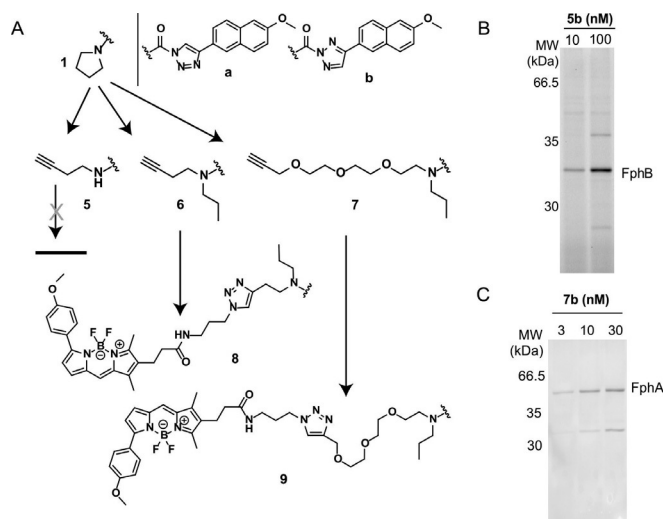


**Figure 2.** Strategy for the design of fluorescent TU activity-based probes and labeling profiles of select clickable intermediates. A) Schematic of ABP design with chemical structures of the clickable probes **5–7a/b** and the corresponding fluorescent probe **8a/b** and **9a/b**. Direct cellular labeling profiles of *S. aureus* Newman cultures with probes B) **5b** and C) **7b**. For direct visualization of labeling with clickable probes in (B,C), labeled proteins were fluorescently tagged by attachment of  $N_3$ -TAMRA by click-chemistry in situ after bacterial lysis and analysed by SDS-PAGE. Data show whole cell extracts excluding secreted proteins in the culture supernatant.

For validation of these probes, we first assessed the cellular selectivity profile of the alkyne probes, labeling live cells with the probe and clicking on a fluorescent tag to probe-labeled targets after bacterial lysis in situ followed by SDS-PAGE analysis. We found that the structural modifications required for installing an alkyne handle had dramatic effects on the selectivity profile of the resulting compounds (Supplementary Results in the Supporting Information, Figure S3) yielding probes that preferentially labeled FphB (**5a/b**, Figure 2B, Figure S3), or were selective for FphA (**7b**, Figure 2C). Introduction of the bodipyTMR fluorophore again produced major changes in the selectivity profile. We then continued with analysis of the fluorescent probes and found that probe **8a** selectively labeled the secreted lipases SAL2 and more weakly SAL1 but did not react with any of the Fph enzymes (Figure 3A and Figure S4) labeled by **6a** (Figure S3C). Reactivity towards SAL1/2 is a shared feature with the parent probe **6a** (Figure S3G). It is conceivable that this selectivity is due to a decreased accessibility of the cell-associated Fph enzymes to the fluorescent probe. While SAL1/2 levels were low when bacteria were harvested from biofilm-like growth on agar, late-stationary-phase cultures of both Newman and USA300 strains show elevated levels of lipase activity. However, while strain Newman only produced detectable levels of SAL1 (Figure S4), USA300 cultures were characterized by high levels of SAL2 activity (present both as the pro-protein and in its matured form; Figure 3A). While probe **8a** is promising as a selective inhibitor and research tool to study the function of SAL1/2 biology, this probe is not suited to provide phenotypic information at the cellular level as its targets are secreted.

Finally, functionalization of the alkyne **7b** with bodipyTMR leading to probe **9b** increased the activity for the secondary target FphE resulting in a loss of the FphA-selectivity seen for **7b**. In contrast, its regioisomer **9a** displayed selectivity for FphE among the cell-associated

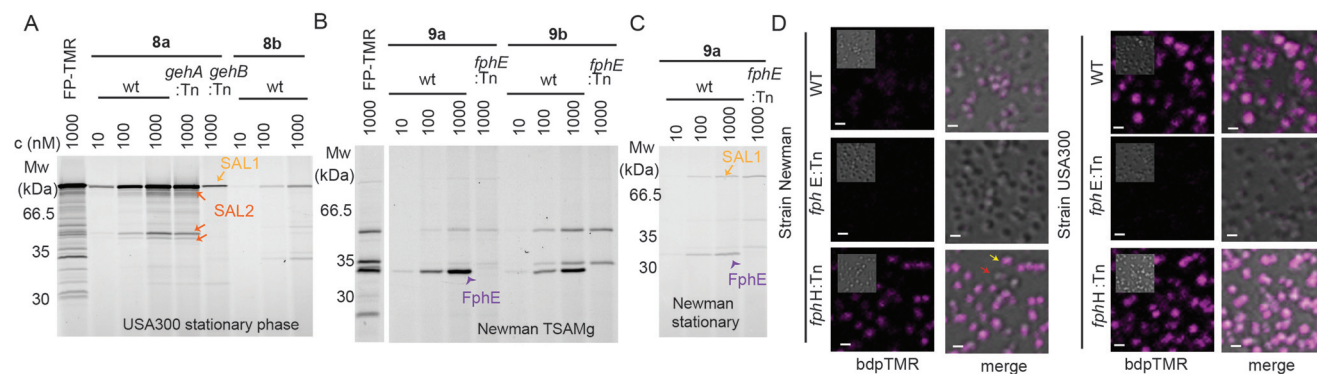


**Figure 3.** Labeling profiles of fluorescent triazole urea probes show selectivity for SAL1/2 or FphE. A) Labeling profile of *S. aureus* USA300 and its transposon mutant (:Tn) cultures in late stationary phase with fluorescent probes **8a**, **8b**, or FP-TMR. Arrows indicate pro-form and matured forms of SAL1 (light orange) and SAL2 (dark orange). B,C) Labeling profile of *S. aureus* Newman and its *fphE* transposon mutant cultures harvested from TSAMg plates (B) or cultures in late stationary phase (C) labelled with fluorescent probes **9a**, **9b**, or FP-TMR. All samples include full cultures with whole cell extracts and secreted culture supernatants. Arrows indicate FphE (purple), SAL1 (orange). D) Confocal micrographs of indicated *S. aureus* wt or transposon mutant cells. Cells were harvested from TSAMg and labelled with 300 nM **9a** in TSB for 30 min, before washing and fixation. Bodipy-TMR fluorescence is shown in magenta. Insets show differential interference contrast images. The red and yellow arrows highlight cells exemplifying the heterogeneity of cellular labeling (red = no or weak labeling, yellow = strong labeling). Scale bar = 1  $\mu$ m.



Fph targets (Figure 3B). Compared to the alkyne **7a** (Figure S3D), for which FphE is also a major target, the fluorescent probe **9a** lost activity against FphA, FphH, and FphF. Probe **9a** also labeled SAL1/2 under stationary-phase conditions in which lipase activities were more abundant (Figures 3C and Figure S4). As SAL1 and SAL2 are secreted, we reasoned that any cellular labeling of **9a** is dependent on FphE. Indeed, confocal fluorescence microscopy experiments with WT and FphE mutant (*fphE:Tn*) cells (harvested from TSAMg plates) revealed that cell-associated labeling of **9a** is specific for FphE (Figure 3D), suggesting FphE activity labeling may be harnessed as a functional parameter for phenotypic characterization of *S. aureus* cells at the single-cell level. Collectively, the data from our probe design efforts indicate that the path from a small inhibitory hit scaffold to the design of a selective ABP is not straightforward and that each functionalization (e.g., with an alkyne or fluorophore) invoked major changes to the selectivity profile with often unanticipated results. Whether these changes are the result of different cellular permeability and target accessibility or due to altered binding affinity to their molecular target remains to be determined.

As a proof-of-principle demonstration of the utility of activity-based probes for phenotypic characterization of bacterial populations, we used probe **9a** to visualize and quantify FphE activity levels and distribution of different *S. aureus* strains under varying culture conditions. Confocal microscopy revealed that Newman cells were only weakly (and heterogeneously) labeled by this probe (Figure 3D). In contrast, USA300 cells gave a much brighter signal. Given the increased FphE-band intensity in the *fphH*-deficient Newman strain (Figure S3D,E), we tested if the FphE-probe **9a** was able to report any corresponding differences in cellular FphE levels by fluorescence microscopy. Indeed, compared to WT cells, probe labeling in Newman *fphH:Tn* cells was highly increased and reached levels comparable to those observed for strain USA300 (Figure 3D). Interestingly, this potential compensatory or phenotypic response to the lack of FphH was not shared by all cells in the population, as individual cells still failed to label with the probe (Figure 3D).

Given these striking differences, we aimed to use probe **9a** to achieve a quantitative read-out of cellular FphE activities under diverse bacterial growth conditions (exponential growth, late stationary phase, and after biofilm-promoting growth on TSAMg) by flow cytometry (Figure 4A,B and Figure S5). In both USA300 and Newman strains, FphE-specific labeling was highest in cells harvested from TSAMg, reaching a mean fluorescence intensity signal of 14.5 or 9.8-fold, respectively, over that observed for the corresponding *fphE:Tn* strain. In USA300, FphE-specific labeling of probe **9a** under these conditions increased by circa 4-fold compared to exponential phase. Throughout all culture stages, USA300 showed higher levels of probe-labeling than strain WT Newman. Of note, in stationary-phase cultures of USA300 a unique subpopulation of circa 25 % of **9a**-positive cells was identified even in the *fphE:Tn* mutant strain (Figure S5). It is tempting to speculate that cells of this subpopulation interact with secreted SAL2, which is highly abundant under this condition and is efficiently labeled by **9a** (Figure S4B).

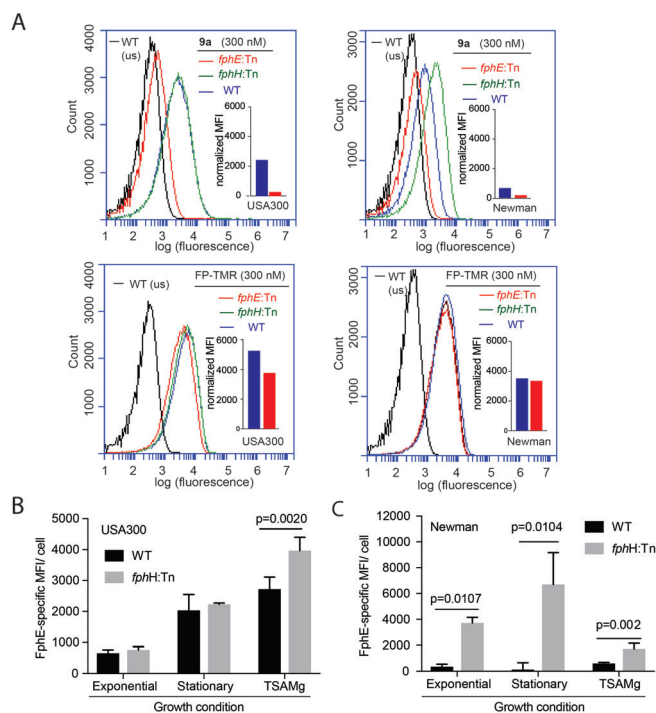


**Figure 4.** Single-cell analysis of *S. aureus* cells labeled with probe **9a** by flow cytometry. A) Representative plot of cellular fluorescence levels for indicated *S. aureus* strains harvested from TSAMg and labelled with **9a** or FP-TMR. Cells were analyzed by flow cytometry (552 nm laser excitation, 586 nm emission filter) after fixation. Insets show corresponding normalized mean fluorescence intensity (MFI) values for wt and transposon mutant strain *fphE:Tn* after subtracting MFI from unstained control samples. B,C) Plots of FphE-specific MFI values of PFA-fixed USA300 (B) or Newman (C) wt or *fphH:Tn* cells labeled with 300 nm of **9a** at indicated growth conditions and analyzed by flow cytometry. Primary MFI values were normalized by subtracting the average MFI value of *fphE:Tn* control samples. Graphs show means  $\pm$  S.D. of three biologically independent culture replicates per condition. Statistical significance was tested by unpaired two-tailed Student's *t*-test.

Activity-dependent labeling of other off-targets (e.g., FphA) or non-specific probe binding would be other conceivable explanations for this cellular phenotype.

In continuation of our phenotypic characterization, we found that Newman *fphH:Tn* showed a statistically significant increase in FphE-specific labeling by **9a** over WT under all culture conditions. Surprisingly, the highest level of labeling in this strain was observed in the late stationary phase (> 10-fold increase; Figure 4C). In contrast, in strain USA300 FphH-deficiency only induced a mild upregulation of FphE activity (ca. 42 %) when grown on TSAMg and had no effect on **9a**-labeling under exponential- and stationary-phase conditions. This large increase in FphE activity in the Newman *fphH:Tn* mutant suggests a particular relevance of FphH activity in the late stationary phase, which merits further investigation. Overall, the quantitative assessment of single cell-labeling by **9a** has revealed that FphE levels are dynamically regulated and are subject to the bacterial growth state and environment in a strain-specific manner. A growth environment-dependent relevance of FphE activity for bacterial physiology would be

consistent with our previous observation that, in a systemic mouse infection model, Newman *fphE*:Tn bacteria showed a mild but statistically significant reduction in only some organs.<sup>[7a]</sup> Importantly, FphE-specific labeling of cells by probe **9a** was also obtained in the context of live imaging (Figure S6). Thus activity-based probe labeling can enable the separation of cells within bacterial populations based on probe-labeling status (e.g., corresponding to single-target or more global enzymatic activities depending on the probe used) by FACS-sorting and downstream functional analysis of purified subpopulations.

In conclusion, we have used the electrophilic TU scaffold to design multiple activity-based probes with selectivity towards distinct bacterial serine hydrolases and enable their selective manipulation and visualization for a variety of potential applications. The use of these probes in molecular imaging studies has provided insight into the regulatory networks underlying these largely uncharacterized enzymes. This study demonstrates that target-selective ABPs are useful tools for single-cell phenotypic characterization of bacteria according to their enzymatic activities and are able to expose a previously hidden level of functional cellular diversity among different bacterial strains and within isogenic populations. Future studies will address the correlation of such cellular phenotypes with clinically relevant parameters such as virulence, metabolic status, or antibiotic resistance parameters.

## Acknowledgements

This work was supported by a National Institutes of Health grant R01 EB026332 (to M.B.), a China Scholarship Council fellowship No. 201604910274 (to L.C.), a Youth Innovation Promotion Association of the Chinese Academy of Sciences grant No.2017329 (to L.C.), and a German Research Foundation (DFG) postdoctoral research fellowship (LE3289/1-1 to C.S.L.). L.J.K. received support from Stanford ChEM-H Chemistry/Biology Interface Predoctoral Training Program, Stanford Molecular Pharmacology Training Grant, and a Stanford Graduate Fellowship. We thank Benjamin Cravatt (The Scripps Research Institute) for providing the triazole urea screening library. We are grateful to Jessica Sheldon and Eric Skaar (Vanderbilt University) for *S. aureus* transposon mutant strains.

## Conflict of interest

The authors declare no conflict of interest.

**Keywords:** activity-based probes · enzymes · molecular imaging · protein profiling · single-cell analysis

**How to cite:** *Angew. Chem. Int. Ed.* **2019**, *58*, 5643–5647  
*Angew. Chem.* **2019**, *131*, 5699–5703

- [1] D. E. Moormeier, K. W. Bayles, *Mol. Microbiol.* **2017**, *104*, 365–376.
- [2] K. Lewis, *Annu. Rev. Microbiol.* **2010**, *64*, 357–372.
- [3] O. M. El-Halfawy, M. A. Valvano, *Clin. Microbiol. Rev.* **2015**, *28*, 191–207.
- [4] a) M. Hecker, D. Becher, S. Fuchs, S. Engelmann, *Int. J. Med. Microbiol.* **2010**, *300*, 76–87; b) R. Thänert, O. Goldmann, A. Beineke, E. Medina, *Nat. Commun.* **2017**, *8*, 14268; c) X. Tan, N. Qin, C. Wu, J. Sheng, R. Yang, B. Zheng, Z. Ma, L. Liu, X. Peng, A. Jia, *Sci. Rep.* **2015**, *5*, 11997; d) A. S. Attia, J. E. Cassat, S. O. Aranmolate, L. J. Zimmerman, K. L. Boyd, E. P. Skaar, *Pathog. Dis.* **2013**, *69*, 36–48.
- [5] a) Y. Liu, M. P. Patricelli, B. F. Cravatt, *Proc. Natl. Acad. Sci. USA* **1999**, *96*, 14694–14699; b) E. J. van Rooden, B. I. Florea, H. Deng, M. P. Baggelaar, A. C. M. van Esbroeck, J. Zhou, H. S. Overkleeft, M. van der Stelt, *Nat. Protoc.* **2018**, *13*, 752–767.
- [6] a) G. Blum, S. R. Mullins, K. Keren, M. Fonovic, C. Jedeszko, M. J. Rice, B. F. Sloane, M. Bogoy, *Nat. Chem. Biol.* **2005**, *1*, 203–209; b) G. Blum, G. von Degenfeld, M. J. Merchant, H. M. Blau, M. Bogoy, *Nat. Chem. Biol.* **2007**, *3*, 668–677.
- [7] a) C. S. Lentz, J. R. Sheldon, L. A. Crawford, R. Cooper, M. Garland, M. R. Amieva, E. Weerapana, E. P. Skaar, M. Bogoy, *Nat. Chem. Biol.* **2018**, *14*, 609–617; b) L. E. Sanman, W. A. van der Linden, M. Verdoes, M. Bogoy, *Cell Chem. Biol.* **2016**, *23*, 793–804; c) P. Kasperkiewicz, Y. Altman, M. D'Angelo, G. S. Salvesen, M. Drag, *J. Am. Chem. Soc.* **2017**, *139*, 10115–10125; d) M. Poreba, W. Rut, M. Vizovisek, K. Groborz, P. Kasperkiewicz, D. Finlay, K. Vuori, D. Turk, B. Turk, G. S. Salvesen, M. Drag, *Chem. Sci.* **2018**, *9*, 2113–2129.
- [8] a) J. Rollof, S. A. Hedstrom, P. Nilsson-Ehle, *Biochim. Biophys. Acta Lipids Lipid Metab.* **1987**, *921*, 364–369; b) B. Cadieux, V. Vijayakumaran, M. A. Bernards, M. J. McGavin, D. E. Heinrichs, *J. Bacteriol.* **2014**, *196*, 4044–4056.
- [9] a) A. Adibekian, B. R. Martin, C. Wang, K. L. Hsu, D. A. Bachovchin, S. Niessen, H. Hoover, B. F. Cravatt, *Nat. Chem. Biol.* **2011**, *7*, 469–478; b) K. L. Hsu, K. Tsuboi, J. W. Chang, L. R. Whitby, A. E. Speers, H. Pugh, B. F. Cravatt, *J. Med. Chem.* **2013**, *56*, 8270–8279; c) K. L. Hsu, K. Tsuboi, L. R. Whitby, A. E. Speers, H. Pugh, J. Inloes, B. F. Cravatt, *J. Med. Chem.* **2013**, *56*, 8257–8269.
- [10] E. J. van Rooden, M. Kohsiek, R. Kreekel, A. C. M. van Esbroeck, A. van den Nieuwendijk, A. P. A. Janssen, R. van den Berg, H. S. Overkleeft, M. van der Stelt, *Chem. Asian J.* **2019**, *14*, 3491–3500.
- [11] G. Koch, A. Yepes, K. U. Forstner, C. Wermser, S. T. Stengel, J. Modamio, K. Ohlsen, K. R. Foster, D. Lopez, *Cell* **2014**, *158*, 1060–1071.

Manuscript received: January 14, 2019

Revised manuscript received: February 1, 2019

Accepted manuscript online: February 15, 2019

Version of record online: March 22, 2019